High-Resolution Waveguide THz Spectroscopy of Biological Molecules

N. Laman,* S. Sree Harsha,* D. Grischkowsky,* and Joseph S. Melinger†
*School of Electrical and Computer Engineering, Oklahoma State University, Stillwater, Oklahoma; and †Naval Research Laboratory, Electronics Science and Technology Division, Code 6812, Washington, District of Columbia

ABSTRACT Low-frequency vibrational modes of biological molecules consist of intramolecular modes, which are dependent on the molecule as a whole, as well as intermolecular modes, which arise from hydrogen-bonding interactions and van der Waals forces. Vibrational modes thus contain important information about conformation dynamics of biological molecules, and can also be used for identification purposes. However, conventional Fourier transform infrared spectroscopy and terahertz time-domain spectroscopy (THz-TDS) often result in broad, overlapping features that are difficult to distinguish. The technique of waveguide THz-TDS has been recently developed, resulting in sharper features. For this technique, an ordered polycrystalline film of the molecule is formed on a metal sample plate. This plate is incorporated into a metal parallel-plate waveguide and probed via waveguide THz-TDS. The planar order of the film reduces the inhomogeneous broadening, and cooling of the samples to 77K reduces the homogenous broadening. This combination results in the line-narrowing of THz vibrational modes, in some cases to an unprecedented degree. Here, this technique has been demonstrated with seven small biological molecules, thymine, deoxycytidine, adenosine, D-glucose, tryptophan, glycine, and L-alanine. The successful demonstration of this technique shows the possibilities and promise for future studies of internal vibrational modes of large biological molecules.

INTRODUCTION

Spectroscopy is a powerful technique for measuring, analyzing, and identifying molecules. The absorption of electromagnetic radiation at different frequency ranges corresponds to different physical processes and reveals information about those processes. For example, in the infrared region, absorption corresponds to motions of nuclei within the molecule. Frequencies in the near- and mid-infrared correspond to stretching or bending motions of individual bonds in the molecule, involving small masses and relatively strong potentials. In contrast, frequencies in the far-infrared and THz (~0.3–6 THz, or 10–200 cm^{-1}) ranges correspond to motions of the entire molecular structure, involving relatively large masses and relatively shallow potentials. Different molecules will vibrate in different characteristic ways and at different characteristic frequencies. These motions are often referred to as vibrational modes and are sensitive to the molecule as a whole. These modes are typically identified via their frequencies. Generally, in spectroscopy, broad, overlapping absorption features can obscure information that subsequently can be revealed if the spectral width of these features is reduced via precise, high-resolution measurements.

Vibrational modes of biological molecules are important for a number of reasons. For example, these modes (1) are sensitive to the conformation of the molecule, as observed in the proteins myoglobin, lysozyme, and bacteriorhodopsin (2,3), and in the chromophore retinal (4). The modes have also been shown to be affected by hydration (5–7), oxidation (8), and ligand binding (9). Particularly strong excitations of vibrational modes can lead to conformational changes (10). In addition, vibrational modes have been linked to chemical reactions in myoglobin (11), as well as biological reactions such as the oxygen acceptance of hemoglobin (12) and the primary event of vision (13).

Due to their delocalized nature, low-frequency vibrational modes are strongly affected by the size and long-range order of the molecule. Small biological molecules (molecular weight <300) such as nucleosides (14–21), amino acids (22–28), and sugars (5,29–31) tend to have distinct, relatively isolated features. Small polymers of these molecules (500 < molecular weight < 2000) such as oligopeptides have a larger number of modes that tend to increase in number and overlap with increasing polymer length (32,33). Large tandem repeats (molecular weight >5000) of peptides (26,33–35) or nucleosides (36) have some observable features, whereas nonperiodic biological molecules such as DNA (7) and proteins (2,3,6,33) have relatively featureless spectra. In addition, the vibrational modes of large molecules tend to be internal (i.e., intramolecular) in nature, with large groups of atoms moving within the molecule. In contrast, small molecules tend to also have external (i.e., intermolecular) modes, where the entire molecule moves in concert within a crystalline lattice. It is not surprising that these modes are strongly dependent on the crystallinity of the material (37).

Many biological vibrational modes have particularly low frequencies. Specifically, the modes of biological interest have frequencies of 3.45 THz (115 cm^{-1}) for the conformational change of bacteriorhodopsin (10), 1.515 THz (50.5 cm^{-1}) for chemical reactions in myoglobin (11), 1.17 THz (39 cm^{-1}) for the oxygen acceptance of hemoglobin (12) and 1.8 THz (60 cm^{-1}) for the primary event of vision (13).

Submitted May 25, 2007, and accepted for publication September 25, 2007.

Address reprint requests to D. Grischkowsky, School of Electrical and Computer Engineering, Oklahoma State University, Stillwater, OK 74078. E-mail: daniel.grischkowsky@okstate.edu.

Editor: Brian R. Dyer.

0006-3495/08/02/1010/11 $2.00

doi: 10.1529/biophysj.107.113647

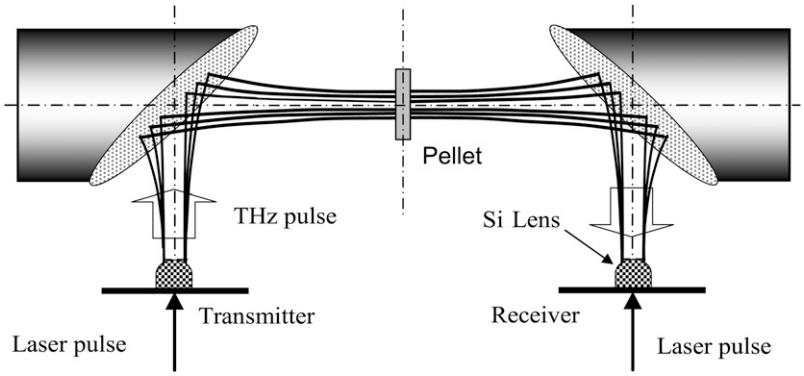

FIGURE 1 Standard THz-TDS.

Historically, absorption lines with frequencies less than ~6 THz (200 cm^{-1}) were difficult to measure with conventional Fourier transform infrared (FTIR) spectroscopy due to the relatively poor performance of thermal sources and detectors in this frequency range. However, since the early 1990s, terahertz time-domain spectroscopy (THz-TDS) has been developed (38), which can exhibit a high signal/noise ratio (S/N) over a frequency range of ~100 GHz to 5 THz. The standard technique for sample preparation in both conventional FTIR spectroscopy and THz-TDS of biological molecules, and organic molecules in general, is to make a mixture of the material in powder form with a transparent host, such as polyethylene, and press the mixture into a pellet, on the order of 1 mm thick with a 1-cm diameter. The transmission spectrum of the pellet is compared to that of a pure host pellet to obtain the absorption spectrum of the sample.

This technique is quite effective and can be used for a very wide range of materials. Previous works have studied pellet samples of a number of biological molecules, including nucleobases and nucleosides (14–21), amino acids (22–28), proteins (2,3,6,33), retinal isomers (4), polypeptides (32–35), sugars (5,29–31), and benzoic and acetylsalicylic acids (39). These cited works have examined a large number of vibrational modes to a high degree. However, for many molecules the resolution of the absorption spectra is limited not by the instrumental resolution, but by the significant inhomogeneous broadening resulting from the disordered polycrystalline sample even at cryogenic temperatures.

In general, disorder in a sample will increase the inhomogeneous broadening. An amorphous sample would have a great deal of broadening and strongly reduced external modes. Ideally, the sample that exhibits the least inhomogeneous broadening would be a defect-free single crystal. In addition, the strength of external modes would increase with the degree of crystallinity. Calculations of the internal modes (and their vibration frequencies) of small isolated molecules such as benzoic acid derivatives can be accomplished relatively easily (40) with software packages such as GAUSSIAN (41) and there has been a great deal of work calculating the internal modes of large molecules such as proteins (42) and DNA (43). However, in the solid state where intermolecular coupling can be strong due to hydrogen bonding, calculation of the low-frequency modes requires more sophisticated modeling and has been accomplished only recently (44,45). Precise, high-resolution, experimental measurements of low-frequency modes of biological molecules in the solid state will lead to better modeling and hence better understanding of these molecules. For example, understanding the role of hydrogen bonding in a crystalline solid may provide better insight on the role of hydrogen bonding in polymers of these biological molecules. In addition, more precise measurements can lead to more accurate identification of a test material.

Our group has recently developed a spectroscopic technique, based on the use of single-mode metal parallel-plate waveguides (46–48), which allows one to easily measure ordered polycrystalline thin films. This technique, which is entitled waveguide THz-TDS and is described in more detail below, can measure vibrational lines of solid polycrystalline samples, with the precision approaching that of a single crystal (48).

In this article, we apply the technique of waveguide THz-TDS to obtain high-resolution THz absorption spectra of many biological molecules. This includes the nucleobase thymine, the nucleoside adenosine, the deoxynucleoside deoxycytidine, the sugar D-glucose, and the amino acids tryptophan, glycine, and L-alanine. These materials were chosen to include a broad sampling of important biological molecules. Adenosine is one of the constituent components of both RNA and ATP, which are necessary for protein synthesis and metabolism, respectively. Both deoxycytidine and

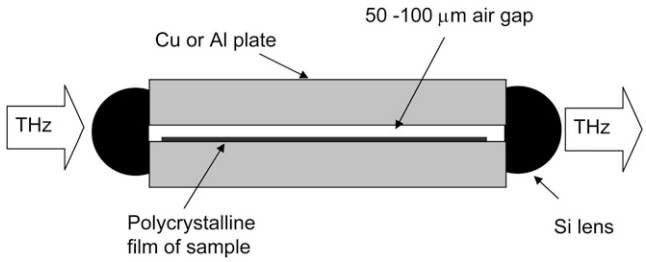

FIGURE 2 Parallel-plate waveguide.

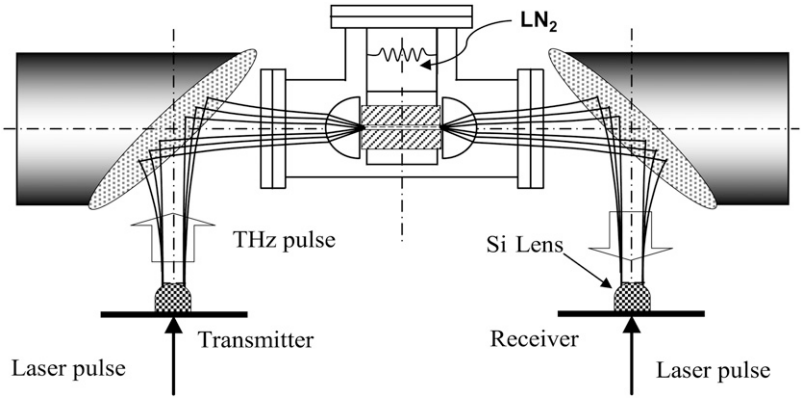

FIGURE 3 Waveguide THz-TDS.

thymine are constituent components of DNA and act as letters of the ''genetic code'' (with and without the ribose group, respectively). D-glucose is the most prevalent biological molecule in nature and is a source of energy and a metabolic intermediate. Tryptophan, glycine, and L-alanine are amino acids and therefore are constituent parts of proteins. In particular, glycine is the smallest amino acid and can act as a destabilizer of the α-helix.

MATERIALS AND METHODS

THz-TDS is comprised of a pair of photoconductive antennae, acting as a THz transmitter and receiver, gated by an ultrafast laser. For standard THz-TDS, the pellet is placed in the collimated THz beam between the THz transmitter and receiver, as shown in Fig. 1, and the transmitted THz signal is compared to that of a pure host pellet. The corresponding amplitude spectra are obtained by numerical Fourier transforms of the measured temporal THz pulses. The instrumental frequency resolution is given by the inverse of the total temporal length of the scan. In general, absorption features sharpen when the sample pellet is cooled to cryogenic temperatures due to a reduction of the homogeneous broadening. Cooling also tends to blue-shift absorption features due to an increase of the intermolecular potential.

Waveguide THz-TDS (46–48) uses metal parallel-plate waveguides (48) comprised of two metal plates separated by a small (50–100 μm) air gap. These are similar to parallel-plate waveguides used for microwave applications, but with the dimensions reduced by approximately a factor of 100 to correspond to the reduced wavelength (1 THz corresponds to a wavelength of 300 μm). Due to the subwavelength size of the gap, the THz pulse propagates in a single transverse electromagnetic mode, exhibiting very little group velocity dispersion. THz is coupled in and out of the waveguide via high-resistivity Si cylindrical lenses. Despite the loss due to the subwavelength gap and reflections from the Si lenses, one can achieve substantial transmission through these waveguides. Typical amplitude transmission of a Cu waveguide with a 50-μm gap is ~20%.

To use the waveguide for spectroscopy, it is opened and the molecular sample is deposited on one of the plates. Different film preparation techniques, such as drop-casting or sublimation, are employed to obtain an ordered polycrystalline film. This planar order (relative to both the metal waveguide plate surface and the THz polarization) is a key component of our technique, as it strongly reduces the inhomogeneous broadening. The waveguide is reassembled as shown in Fig. 2 and then placed in a vacuum chamber with straight-through optical access and in contact with a liquid nitrogen container. The whole assembly is then placed in the THz-TDS system as shown in Fig. 3. Cooling of the waveguide to 77 K strongly reduces the homogeneous broadening. Combined with the reduced inhomogeneous broadening described above, this can result in unprecedented narrow THz absorption lines associated with vibrational modes.

The metal parallel-plate waveguide is an ideal structure to study the ordered polycrystalline film, because the subwavelength confinement of the THz leads to a strong interaction between the THz electric field and the metal plates over a distance of centimeters (49). This increased interaction length results in a sensitivity enhancement proportional to the ratio of the waveguide length to the separation between the plates (50). This sensitivity enhancement was used previously to measure nanometer water layers deposited in situ (46). For our experiments, the sensitivity enhancement is on the order of 100 for any thin layer, independent of obtaining an ordered polycrystalline film.

Most of the biological molecular samples were prepared by drop-casting solutions onto aluminum or copper plates, although some required sublimation. One of the challenges in this work is to find an appropriate

TABLE 1 Summary of absorption line frequencies and amplitude absorbance line widths at 77 K

Material*	Film preparation	Absorption lines at 77 K†
Deoxycytidine (MW 227)	Water drop-cast (12 mg/ml)	1.62 THz (0.02 THz), 1.78 (0.03), 2.09 (0.05), 2.17(0.03), 2.30 (0.04), 2.48 (0.04), 2.76 (0.04)
Adenosine (MW 267)	Sublimation	2.10 THz (0.06 THz), 2.27 (0.02), 2.97 (0.05), 3.16 (0.05)
Thymine (MW 126)	Water drop-cast (10 mg/ml)	0.84 THz (0.09 THz), 0.99 (0.08), 2.03 (0.06), 2.5 (0.2)
D-glucose (MW 180)	Sublimation	1.89 THz (0.05 THz), 2.11 (0.04), 2.57 (0.06)
L-alanine (MW 89)	Water drop-cast (10 mg/ml)	1.43 THz (0.08 THz), 1.65 (0.05), 1.96 (0.04), 2.01 (0.03), 2.25 (0.009), 2.62 (0.03)
Glycine (MW 75)	Water drop-cast (10 mg/ml)	0.75 THz (0.15 THz), 1.27 (0.08), 1.95 (0.06), 2.11 (0.12), 2.39 (0.09), 2.85 (0.12)
Tryptophan (MW 204)	Methanol drop-cast (3 mg/ml)	1.44 THz (0.09 THz), 1.77 (0.08), 2.14 (0.12), 2.32 (0.11)

*MW, molecular weight.
†Values in parentheses are absorbance FWHM linewidths given in THz.

method to acquire an ordered polycrystalline film. Initially, we prepare a film by drop-casting from a water solution onto an optically polished, plasma-cleaned copper or aluminum waveguide plate. Copper is generally preferable because its high conductivity results in larger transmission through the waveguides. If this initial attempt does not result in a visible crystal structure, then attempts are made with different solvents and substrates. Failing this, a film is deposited via sublimation. Here, a small amount of the molecular powder is placed in an evacuated chamber and heated to just below the melting point, with the waveguide plate placed a few centimeters above the powder and in thermal contact with a reservoir of room-temperature water. The powder sublimes and recrystallizes on the relatively cold surface of the waveguide plate, forming an ordered polycrystalline film. It has been our experience that the formation of the polycrystalline film of nucleosides, deoxynucleosides, or sugars is sensitive to environmental conditions. The full polycrystalline film may not appear until days after the drop-cast or sublimation. This may be due to these flexible materials slowly reaching the complex hydrogen-bonded network of the crystalline state. In contrast, the formation of polycrystalline films of amino acids and of the nucleobase thymine is relatively insensitive to environmental conditions and the film appears a few hours after the initial drop-cast. With the exception of deoxycytidine, all of the films were dried at room temperature and at ambient humidity (~30–60% relative humidity).

The metal plates used in this series of experiments have dimensions of 27.9 mm (width) × 30.5 mm (length) × 9.5 mm (thickness), and the plate separation was kept at 50 μm in the experiments, with the exception of those for thymine, where the plate separation was increased to 100 μm. In all cases, the amplitude spectrum of the transmitted THz was determined by the numerical Fourier transform of the measured transmitted THz pulse. For glycine, tryptophan, and D-glucose, the measured temporal scan length (i.e., the length of the full measurement of the transmitted temporal signal) was 33.36 ps, whereas for thymine, adenosine, and L-alanine the scan length was 66.71 ps long and for deoxycytidine it was 100.07 ps long, which corresponds to effective instrument resolution of 1/33.36 ps = 30 GHz, 15 GHz, and 10 GHz, respectively. With respect to this situation, the duration of the experimental measurement is determined by the delay time at which the sample's oscillatory signal disappears into the noise floor, at the delay where S/N ≈ 1. Scan lengths longer than this merely increase the spectral noise, even though the instrument resolution is increased. The 33.36-ps and 66.71-ps-long scans were zero-padded by a factor of 2 before the Fourier transform. Zero-padding performs an interpolation in the frequency domain; it does not change the linewidth or increase the frequency resolution.

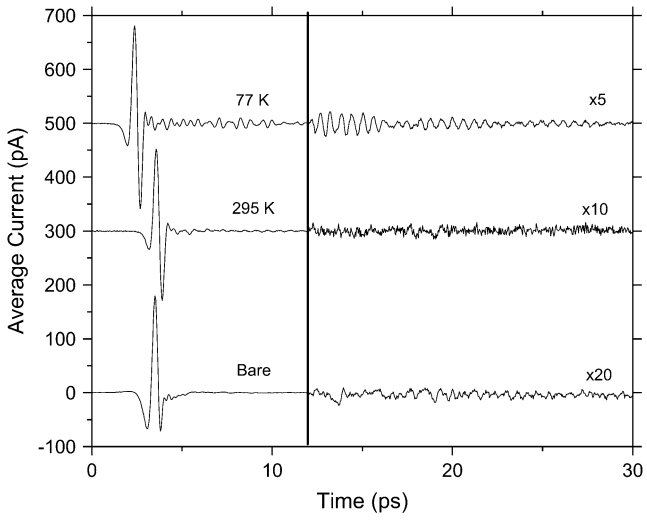

FIGURE 4 Measured transmitted THz pulses for deoxycytidine waveguide and for reassembled bare Cu waveguide. Signals for deoxycytidine waveguide are offset for clarity. Scale is expanded by the indicated factor after 12 ps. The complete measured signal at 77 K is 100.07 ps long.

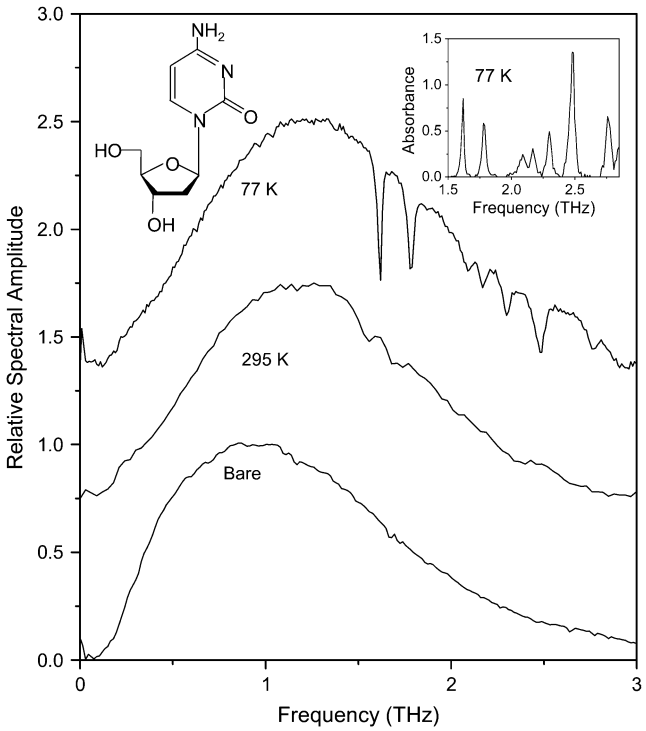

FIGURE 5 Corresponding amplitude spectra for the THz pulses (Fig. 4) transmitted through bare waveguide and waveguide with deoxycytidine film. Spectra for deoxycytidine film are offset for clarity. (*Inset*) Absorbance spectrum at 77 K. Spectrum at 295 K is normalized to unity.

Due to small differences in the transmission of the waveguide upon disassembly, reassembly, and realignment of the lenses, it can be difficult to measure an unambiguous reference spectrum, particularly at low temperature. For this reason, we estimate a reference by choosing points in the transmission spectra that are far from any sharp absorption features, and then fitting those points to a spline. The absorbance is then calculated from this smooth reference and the transmitted amplitude spectrum, $A(\omega)_R$ and $A(\omega)_T$, respectively; the amplitude absorbance shown in the figures is given by

TABLE 2 Comparison of absorption line frequencies for deoxycytidine in this study and two others

This work 77 K	Fischer et al. (14) 10 K	Li et al. (16) 10 K
	0.85 (0.05)	
	1.55 (0.07)	1.54 (n.o.)
1.62 (0.02)		
1.78 (0.03)	1.75 (0.10)	
2.09 (0.05)	2.09 (0.13)	
2.17 (0.03)		
2.30 (0.04)	2.35 (0.09)	
2.48 (0.04)	2.50 (0.06)	2.43 (n.o.)
2.76 (0.04)		2.76 (n.o.)
	2.82 (0.06)	

Values in parentheses are the FWHM linewidths. Both frequencies and linewidths are given in THz. Frequencies for Fischer et al. (14) and linewidths for both references are estimated from corresponding figure. n.o., linewidths not obtainable.

absorbance $= -\ln[A(\omega)_T/A(\omega)_R]$. Although the absorbance amplitude is only estimated through this method, the center-line frequencies and linewidths can be precisely measured. The absorption-line frequencies and amplitude-absorbance linewidths at 77 K for all of the materials are summarized in Table 1.

RESULTS AND DISCUSSION

Deoxycytidine

The deoxycytidine film was prepared by drop-casting a 12 mg/ml solution in deionized (DI) water onto an optically polished, plasma-cleaned Cu waveguide plate. The transmitted THz pulse through the corresponding waveguide is shown in Fig. 4. The shift to earlier times at cooler temperatures is due to the temperature-dependent refractive index of the Si lenses (51). The observed ringing in the time domain corresponds to sharp features in the corresponding transmission spectrum obtained by a numerical Fourier transform of the complete pulse measurements, as shown in Figs. 4 and 5. The absorption lines sharpen significantly under cooling, with seven observed absorption lines at 77 K and linewidths ranging from 20 to 50 GHz. The appearance of these lines critically depends on the surface morphology, implying that the lines are related to intermolecular as opposed to intramolecular modes. In particular, the morphology of the film depends strongly on the humidity, with the best results resulting from the film drying in a high-humidity (~80%) environment.

Deoxycytidine has been studied previously in pellet form at 10 K by Fischer et al. (14) and Li et al. (16). The absorption-line frequencies observed in these studies are summarized in Table 2. Of the seven lines observed in the work described here, two (at 2.48 THz and 2.76 THz) were observed by Li et al. (16) and identified as lattice modes. Fischer et al. (14) identified seven lines in our measurable bandwidth, of which three (at 1.75 THz, 2.09 THz, and 2.5 THz) agree with our observations, whereas two (at 0.85 THz and 1.55 THz) are not observable in our data. The remaining two lines (at 2.35 THz and 2.82 THz) may correspond to our observed lines at 2.30 and 2.76 THz, respectively. It would appear that the broad (~130-GHz) feature observed by Fischer et al. (14) at 2.09 THz at 10 K can be resolved into a doublet through the power of our technique. The discrepancies between our results and those of Fischer et al. (14) and Li et al. (16), and between the results of the latter two studies, can be attributed to the dependence of intermolecular absorption lines on the polycrystalline structure. In addition, the relative strengths of our observed absorption lines differ from those in Fischer et al. (14) and Li et al. (16). This can be attributed to the projection of the dipole moments of our ordered crystals onto the electric field, as opposed to an average over projections from randomly oriented crystals.

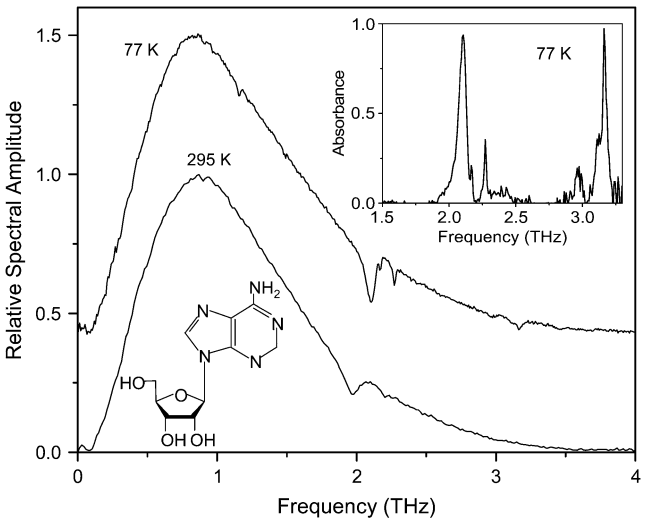

FIGURE 6 Spectra of THz transmitted through waveguide with adenosine film. Spectrum at 77 K is offset for clarity. (*Inset*) Absorbance spectrum at 77 K. Spectrum at 295 K is normalized to unity.

Adenosine

The adenosine film was prepared by sublimation onto an optically polished, plasma-cleaned Cu waveguide plate. The Cu plate was kept in thermal contact with a room-temperature water reservoir during the sublimation. The transmission spectrum of the corresponding waveguide is shown in Fig. 6.

TABLE 3 Summary of absorption line frequencies and FWHM linewidths for adenosine in this and several other studies

Nishizawa et al. (19) 300 K	Bailey et al. (20) 300 K	Lee et al. (18) 300 K	Lee et al. (18) 150 K	This study 77 K	Lee et al. (18) 20 K	Shen et al. (21) 4 K
0.77 (0.07)						
	1.53 (n.o.)					
	1.71 (n.o.)					1.17 (n.o.)
1.96 (0.18)	1.95 (0.07)	1.95 (0.2)	2.05 (n.o.)	2.10 (0.06)	2.14 (0.07)	2.12 (0.08)
2.21 (0.2)				2.27 (0.02)		2.28 (0.03)
			2.32 (n.o.)		2.39 (0.1)	2.45 (0.02)
2.77 (n.o.)				2.97 (0.05)		3.02 (0.02)
3.03 (0.13)		3.01 (0.1)	3.14 (n.o.)	3.16 (0.05)	3.19 (0.1)	3.20 (0.05)
3.33 (0.14)		3.34 (0.2)	3.45 (n.o.)		3.45 (0.1)	

FWHM linewidths are shown in parentheses. Both frequencies and linewidths are given in THz. Linewidths for column 1–4 and 6 (18–21) are estimated from the corresponding figures. n.o., linewidths not obtainable.

There is significant sharpening in the absorption lines under cooling, with four observed lines at 77 K and linewidths ranging from 20 to 60 GHz. The lines are dependent on the crystal morphology, as the lines are not observed with the different morphology resulting from a drop-cast from an ammonium hydroxide solution onto plates protected by a thin film of mylar.

A summary of our observed lines for adenosine compared to the lines observed in four other studies (18–21) is shown in Table 3. The 2.10-THz line was previously observed by references 18 through 21, whereas the 2.27- and 2.97-THz lines were observed by Nishizawa et al. (19) and Shen et al. (21), and the 3.16-THz line was observed by references Lee et al. (18), Nishizawa et al. (19), and Shen et al. (21). Lee et al. (18) attribute all of the lines in this frequency range to lattice modes, whereas Bailey et al. (20) attribute the 2.10-THz line to torsions of the ribose residue.

Thymine

The thymine film was prepared by drop-casting a 10 mg/ml DI water solution onto an optically polished, plasma-cleaned Cu waveguide plate. Unlike the other molecules in this study, the resulting film for thymine is >50 μm thick, requiring the use of a 100-μm gap between the waveguide plates. The spectrum of the transmitted THz pulse through this waveguide is shown in Fig. 7. There are four visible absorption lines at 0.84, 0.99, 2.03, and 2.5 THz. The two higher-frequency lines have been observed previously in Fischer et al. (14). The two lower-frequency features appear as a single feature at 295 K, but split during cooling. It would appear that one feature slightly red-shifts, whereas the other feature blue-shifts. The blue-shifting of absorption lines can be explained by a steepening of the intermolecular potential along with the anharmonicity of the modes. In contrast, the red-shifting is more difficult to explain, though it may be associated with van der Waals forces influencing hydrogen bonds (31). When the concentration of the drop-cast solution is lowered, the crystal morphology changes and the lower-frequency features disappear. This would indicate that these features are due to external modes. A recent calculation of the vibrational modes of a thymine crystal (44) with a $P2_1/c$ space group predicts the existence of the two higher-frequency lines, and that all of the vibrational modes in our observable frequency range will be external in nature.

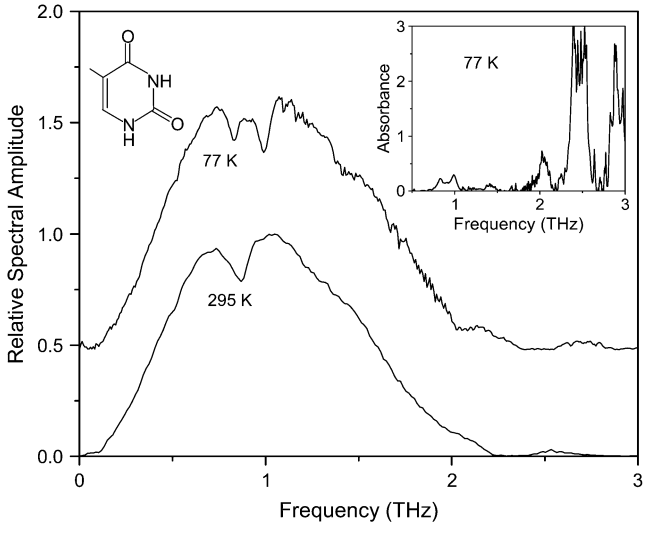

FIGURE 7 Spectra of THz transmitted through waveguide with thymine film. Spectrum at 77 K is offset for clarity. (*Inset*) Absorbance spectrum at 77 K. Spectrum at 295 K is normalized to unity.

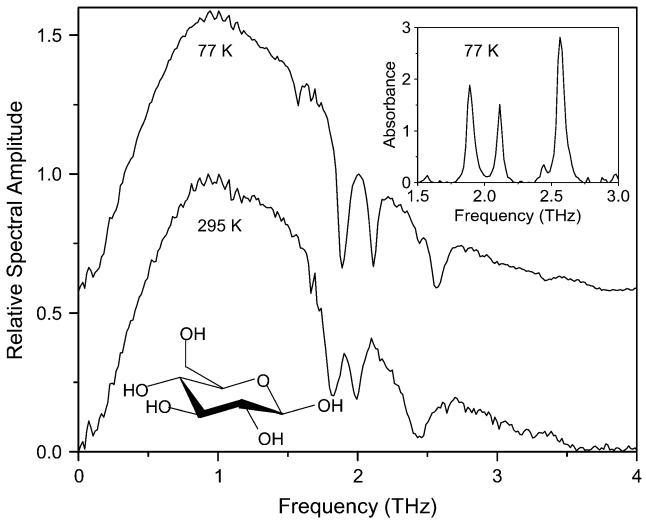

FIGURE 8 Spectra of THz transmitted through waveguide with D-glucose film. Spectrum at 77 K is offset for clarity. (*Inset*) Absorbance spectrum at 77 K. Spectrum at 295 K is normalized to unity.

D-glucose

The D-glucose film was prepared by sublimation onto an optically polished, water-cooled Al waveguide plate. The spectrum of the transmitted THz pulse through the corresponding waveguide is seen in Fig. 8. Three absorption lines were observed at 1.89, 2.11, and 2.57 THz. Although our observed absorption features do not agree with previous results on dry D-glucose (29–31), they do agree with the absorption features observed with D-glucose monohydrate (5). Our hypothesis is that water is incorporated into our D-glucose film after sublimation. Indeed, the visible crystal structure appears on the timescale of several hours in ambient air (~45% humidity) after the sublimation (as did the adenosine crystals studied above).

L-alanine

The L-alanine film was prepared by drop-casting a 10 mg/ml DI water solution onto an optically polished, plasma-cleaned

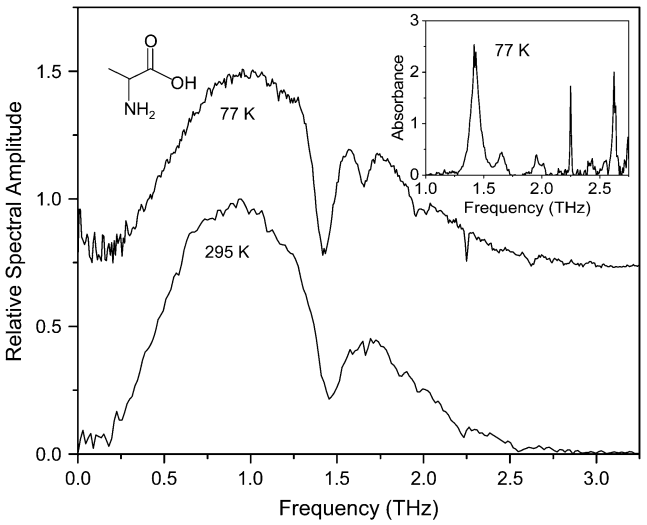

FIGURE 9 Spectra of THz transmitted through waveguide with L-alanine film. Spectrum at 77 K is offset for clarity. (*Inset*) Absorbance spectrum at 77 K. Spectrum at 295 K is normalized to unity.

Cu waveguide plate. The spectrum of the transmitted THz pulse through the corresponding waveguide is seen in Fig. 9. Six absorption lines were observed, with one line (at 2.25 THz) being particularly narrow with a full width at half-maximum (FWHM) line width of 9 GHz (0.3 cm^{-1}). This linewidth is approximately an order of magnitude less than those previously reported for pellets (22) and transverse measurements of films grown on Si substrates (23–25). Moreover, the linewidth we observed is limited by the frequency resolution; the intrinsic linewidth may be even narrower. The lines at 2.25 and 2.62 THz have also been reported previously (22–25), but the four lowest frequency modes (1.43, 1.65, 1.96, and 2.01 THz) have not. It is our hypothesis that the four lowest frequency modes are external modes that are only observable for our ordered polycrystalline film. Given that L-alanine crystallizes in the D_2^4 space group with 4 molecules/unit cell and 12 infrared active lattice modes, it is not surprising that we see a large number of external modes. When the L-alanine film was prepared by drop-casting the same solution onto an optically polished, plasma-cleaned Al plate, a very different film morphology was visible and no absorption lines were observed at 295 K and 77 K. Optical micrographs of the different crystal morphologies are shown in Fig. 10. Note that these morphological differences are reproducible. The dependence of the crystal morphology on the metal substrate is considered to be related to the chemical interaction between the metal and the first layer of the deposited film. The morphology of subsequent layers of the film is then dependent on the morphology of this first layer.

To investigate the alternative possibility of the different morphologies being due to Cu ions, plasma-cleaned Cu foil was placed in an L-alanine/water solution and left for several hours. This solution was then drop-cast onto an optically polished, plasma-cleaned Al plate, and the resulting polycrystalline film was shown to be similar in both morphology and THz spectrum to that of an equivalent solution (without the Cu foil) drop-cast on an equivalent Al plate. This suggests that the differences in morphology are due to the chemical/metal surface interaction and not to metallic ions in the solution. It should be noted that our previous work with nonbiological materials such as 1,2-dicyanobenzene (47) and tetracyanoquinodimethane (48) has not shown this dependence on the metal substrate composition.

Glycine

The glycine film was prepared by drop-casting a 10 mg/ml DI water solution onto an optically polished, plasma-cleaned Cu waveguide plate. The spectra of the transmitted THz pulse through the waveguide with the glycine film are seen in Fig. 11. There are six visible absorption lines. The lowest frequency line (0.75 THz) is relatively broad (150 GHz FWHM). This line also differs from most of the other lines in this study by red-shifting as it is cooled to 77 K. This feature is particularly visible as it shifts back during the subsequent warm-up. The degree of red-shifting is considerably stronger for this feature compared to the lowest-frequency feature of the thymine film. It should be noted that previous observations of red-shifting vibrational modes (31) were also at

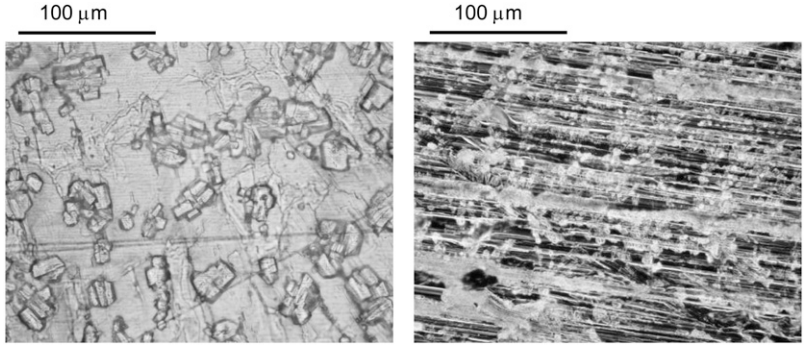

FIGURE 10 Optical micrographs of L-alanine polycrystalline films. (*Left*) Film resulting from drop-cast of water solution onto Cu plate. (*Right*) Corresponding drop-cast on Al plate. Micrograph on right is negative for clarity.

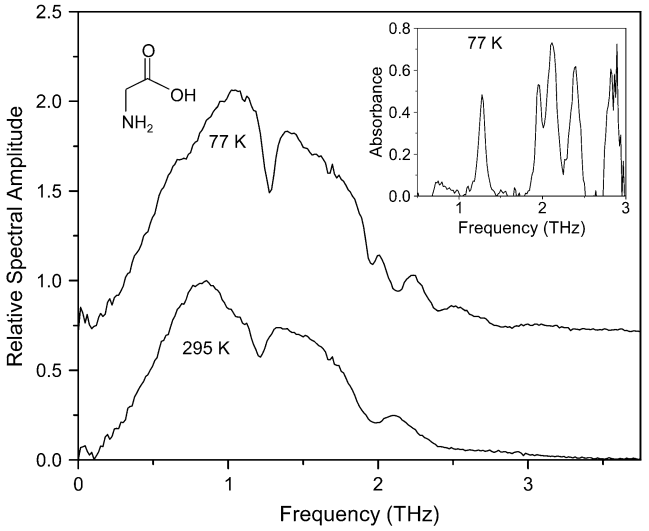

FIGURE 11 Spectra of THz transmitted through waveguide with glycine film. Spectrum at 77 K is offset for clarity. (*Inset*) Absorbance spectrum at 77 K. Spectrum at 295 K is normalized to unity.

particularly low frequencies. The feature around 2 THz at 295 K sharpens significantly when cooled, revealing a doublet (1.95 and 2.11 THz). Shotts and Sievers (33) observed two features at 2.04 THz and 2.75 THz at 4 K, which is somewhat similar to our observed features at 2.11 and 2.85 THz at 77 K, whereas Kutteruf et al. (32) observed two features at 2.67 and 3.11 THz at 298 K and Shi and Wang (27) observed features at 2.4 and 2.7 THz at 298 K. None of these studies reported our observed line at 1.27 THz, although Kutteruf et al. (32) and Shotts and Sievers (33) used FTIR spectroscopy and had a low S/N at this frequency, due to the insufficient low-frequency bandwidth.

As with L-alanine, when the glycine plate is prepared on an optically polished, plasma-cleaned Al plate, a different, reproducible, crystal morphology is observed (see Fig. 12), along with a lack of all but one of the absorption lines (at 1.96 THz). Similar to L-alanine, this second morphology is unaffected by the presence of Cu ions introduced in the solution. Also similar to L-alanine, glycine crystallizes into a space group (C_{2h}^5) with 4 molecules/unit cell and 12 infrared active lattice modes. For these reasons, we consider that these absorption features are associated with external modes. Both L-alanine and glycine have a much smaller molecular weight than the other molecules measured in this work, implying that many of their internal modes are going to be at higher frequencies.

Tryptophan

The tryptophan film was prepared by drop-casting a 3 mg/ml methanol solution onto a brush-finished, plasma-cleaned Al plate. The spectrum of the transmitted THz pulse through the corresponding waveguide is seen in Fig. 13. There are four visible absorption lines at 1.44, 1.77, 2.14, and 2.32 THz. These lines blue-shift only slightly under cooling, but sharpen appreciably, revealing a doublet at higher frequencies. Unlike with most of the other materials in this study, all four absorption features survive when the tryptophan film is prepared using a different method (e.g., drop-cast from a water solution onto either an optically polished or brush-finished Al plate), resulting in a different polycrystalline morphology. Optical micrographs of two of these morphologies are shown in Fig. 14.

The consistency of the spectra implies that the absorption features for tryptophan are due to internal modes. In a previous experimental work on tryptophan (28), the authors found two absorption features at 1.44 and 1.84 THz which were attributed to torsion vibrational modes associated with the chain and the ring of the molecule, respectively. Given the consistency of our observed spectrum and the small blue-shifting upon cooling, it is somewhat surprising that our observed frequency (1.77 THz) of the second absorption line differs from that in Yu et al. (28) (1.84 THz). That study was limited to frequencies of <2.0 THz.

When tryptophan is drop-cast from a water solution onto a copper plate, the different crystal morphology is accompanied by a change in the film color from white to blue, implying the incorporation of Cu ions. This incorporation of Cu ions greatly affects the THz spectrum, with only one strong feature at 0.65 THz. Placing Cu foil in the tryptophan

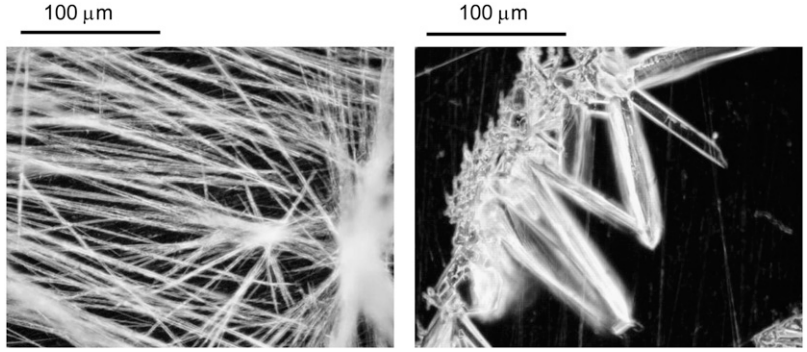

FIGURE 12 Optical micrographs of glycine polycrystalline films. (*Left*) Film resulting from drop-cast of water solution onto Cu plate. (*Right*) Corresponding drop-cast on Al plate. Both micrographs are negative for clarity.

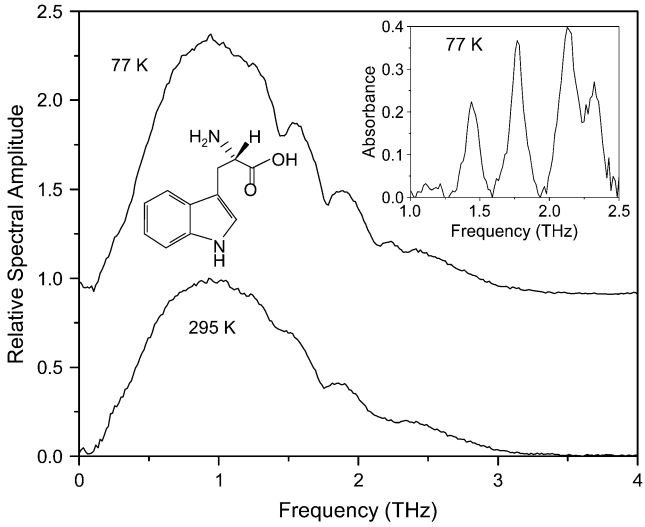

FIGURE 13 Spectra of THz transmitted through waveguide with tryptophan film. Spectrum at 77 K is offset for clarity. (*Inset*) Absorbance spectrum at 77 K. Spectrum at 295 K is normalized to unity.

solution results in the tryptophan coming out of solution and forming a blue deposition on the Cu. This further suggests some chemical interaction between Cu and tryptophan.

CONCLUSIONS

The preceding seven examples show the power of high-resolution waveguide THz spectroscopy applied to the study of biological molecules. The preparation of an ordered polycrystalline film on a metal waveguide plate can significantly reduce the inhomogeneous broadening associated with THz vibrational modes. The subsequent incorporation of the metal plate into a single transverse electromagnetic mode parallel-plate waveguide allows the film to be interrogated by a THz beam with a high sensitivity via a long interaction length. This technique has resulted in unprecedentedly narrow lines even at relatively high temperatures.

Waveguide THz-TDS has demonstrated the complex nature of low-frequency vibrational modes of biological molecules in the solid phase. With the notable exception of tryptophan, the strong dependence of the THz spectra on film morphology indicates that many of the observed modes arise due to strong intermolecular coupling where their transition strengths and linewidths are related to the degree of long-range order. Indeed, for hydrogen-bonded solids a clear distinction between internal (intramolecular) and external (intermolecular) vibrational motion in the THz region may not be possible in many cases (44). The calculation of the physical vibrating motions corresponding to these modes is an ongoing endeavor (44) and may be guided by our more precise measurements.

Not only can narrow lines result in a more precise measurement of the center line frequency, but they also reveal structure that was not previously visible. In addition, narrow lines make the THz absorption spectra of different molecules more distinguishable, which leads to the possibility of using them as ''spectral fingerprints''. Waveguide THz-TDS also requires far less material than conventional THz-TDS using pellet samples (47,48), which is advantageous if one is measuring a toxic or otherwise dangerous material.

The next step in our work is to use more controlled methods for film preparation to generalize our technique to biological molecules for which it is difficult to form an ordered polycrystalline film. One possible method is through the use of patterned self-assembled monolayers (SAMs) (52–54). SAMs of nucleobases have already been achieved on Au (55) and graphite (56). The application of the proper functional groups on the substrate to attract the ribose ring in nucleosides or the 2-deoxyribose ring in deoxynucleosides may enable these materials to form ordered crystalline films.

Now that waveguide THz-TDS has been demonstrated for small biological molecules, the work can be extended to larger biological molecules. One outstanding experimental challenge is the observation of specific vibrational resonances that are associated with the motion of secondary structures. Previous work (2,3,6,33) on disordered proteins has been limited by line-broadening effects. However, oriented films of tandem repeats of peptides (specifically poly(γ-benzyl-L-glutamate)) have been achieved by self-assembly (57) and by

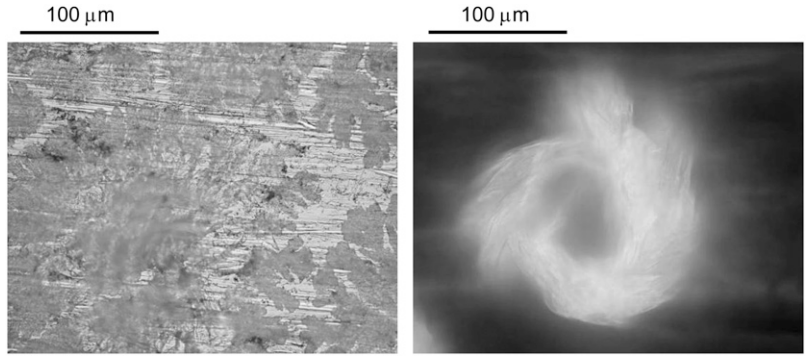

FIGURE 14 Optical micrographs of tryptophan films drop-cast onto brushed Al plates. (*Left*) Film from methanol solution. (*Right*) Film from water solution. Micrograph on right is negative for clarity.

techniques that employ grafting (58) onto substrates. These films are well suited to waveguide THz-TDS due to their large degree of long-range order. It would be illuminating if vibrational modes due to the secondary structure of polypeptides, such as the α-helix and β-sheet, could be observed. Similarly, it has been shown that relatively ordered films of DNA can be formed via SAMs (59). Although ''wild'' DNA has a relatively featureless THz spectrum, tandem repeats of nucleosides would have the required long-range order for waveguide THz-TDS. Precise measurements of these tandem repeats of nucleosides may enlighten the ongoing discussion of charge transport in DNA (60).

We anticipate that controlled preparation of ordered polycrystalline films, coupled with waveguide THz-TDS, will allow one to measure the vibrational modes of biological molecules to an unprecedented degree. These measurements may guide future calculations, which in turn could lead to more understanding about the physical nature of the lowest-order vibrations of these molecules. Furthermore, precise measurements can lead to more accurate ''spectral fingerprints'' for identification purposes. Whereas this study concentrated on external modes for small biological molecules in a crystalline structure, future work will study internal modes for large molecules.

We thank Architha Nath for technical assistance with sample preparation.

This work was supported by the National Science Foundation and the Office of Naval Research.

REFERENCES

1. Chou, K.-C. 1988. Low-frequency collective motion in biomacromolecules and its biological functions. *Biophys. Chem.* 30:3–48.
2. Markelz, A., S. Whitmire, J. Hillebrecht, and R. Birge. 2002. THz time domain spectroscopy of biomolecular conformational modes. *Phys. Med. Biol.* 47:3797–3805.
3. Whitmire, S. E., D. Wolpert, A. G. Markelz, J. R. Hillebrecht, J. Galan, and R. R. Birge. 2003. Protein flexibility and conformational state: a comparison of collective vibrational modes of wild-type and D96N bacteriorhodopsin. *Biophys. J.* 85:1269–1277.
4. Walther, M., B. Fischer, M. Schall, H. Helm, and P. U. Jepsen. 2000. Far-infrared vibrational spectra of all-*trans*, 9-*cis* and 13-*cis* retinal measured by THz time-domain spectroscopy. *Chem. Phys. Lett.* 332:389–395.
5. Liu, H.-B., and X.-C. Zhang. 2006. Dehydration kinetics of D-glucose monohydrate studies using THz time-domain spectroscopy. *Chem. Phys. Lett.* 429:229–233.
6. Knab, J., J.-Y. Chen, and A. Markelz. 2006. Hydration dependence of conformational dielectric relaxation of lysozyme. *Biophys. J.* 90:2576–2581.
7. Kistner, C., A. André, T. Fischer, A. Thoma, C. Janke, A. Bartels, T. Gisler, G. Maret, and T. Dekorsy. 2007. Hydration dynamics of oriented DNA films investigated by time-domain terahertz spectroscopy. *Appl. Phys. Lett.* 90:233902.
8. Chen, J.-Y., J. R. Knab, J. Cerne, and A. G. Markelz. 2005. Large oxidation dependence observed in terahertz dielectric response for cytochrome *c*. *Phys. Rev. E Stat. Nonlin. Soft Matter Phys.* 72:040901.
9. Balog, E., T. Becker, M. Oettl, R. Lechner, R. Daneil, J. Finney, and J. C. Smith. 2004. Direct determination of vibrational density of states change on ligand binding to a protein. *Phys. Rev. Lett.* 93:028103.
10. Xie, A., A. F. G. van der Meer, and R. H. Austin. 2002. Excited-state lifetimes of far-infrared collective modes in proteins. *Phys. Rev. Lett.* 88:018102.
11. Austin, R. H., M. W. Roberson, and P. Mansky. 1989. Far-infrared perturbation of reaction rates in myoglobin at low temperatures. *Phys. Rev. Lett.* 62:1912–1915.
12. Klug, D. D., M. Z. Zgierski, J. S. Tse, Z. Liu, J. R. Kincaid, K. Czarnecki, and R. J. Hemley. 2002. Doming modes and dynamics of model heme compounds. *Proc. Natl. Acad. Sci. USA.* 99:12526–12530.
13. Wang, Q., R. W. Schoenlein, L. A. Peteanu, R. A. Mathies, and C. V. Shank. 1994. Vibrationally coherent photochemistry in the femtosecond primary event of vision. *Science.* 266:422–424.
14. Fischer, B. M., M. Walther, and P. U. Jepsen. 2002. Far-infrared vibrational modes of DNA components studied by terahertz time-domain spectroscopy. *Phys. Med. Biol.* 47:3807–3814.
15. Lee, S. A., M. Schwenker, A. Anderson, and L. Lettress. 2004. Temperature-dependent Raman and infrared spectra of nucleosides. IV–Deoxyadenosine. *J. Raman Spectrosc.* 35:324–331.
16. Li, J., S. A. Lee, A. Anderson, L. Lettress, R. H. Griffey, and V. Mohan. 2003. Temperature-dependent Raman and infrared spectra of nucleosides. III–Deoxycytidine. *J. Raman Spectrosc.* 34:183–191.
17. Lee, S. A., J. Li, A. Anderson, W. Smith, R. H. Griffey, and V. Mohan. 2001. Temperature-dependent Raman and infrared spectra of nucleosides. II–Cytidine. *J. Raman Spectrosc..* 32:795–802.
18. Lee, S. A., A. Anderson, W. Smith, R. H. Griffey, and V. Mohan. 2000. Temperature-dependent Raman and infrared spectra of nucleosides. Part I–Adenosine. *J. Raman Spectrosc.* 31:891–896.
19. Nishizawa, J.-I., T. Sasaki, K. Suto, T. Tanabe, K. Saito, T. Yamada, and T. Kimura. 2005. THz transmittance measurements of nucleobases and related molecules in the 0.4- to 5.8-THz region using a GaP THz wave generator. *Opt. Commun.* 246:229–239.
20. Bailey, L. E., R. Navarro, and A. Hernanz. 1997. Normal coordinate analysis and vibrational spectra of adenosine. *Biospectroscopy.* 3: 47–59.
21. Shen, Y. C., P. C. Upadhya, E. H. Linfield, and A. G. Davies. 2004. Vibrational spectra of nucleosides studied using terahertz time-domain spectroscopy. *Vib. Spectrosc..* 35:111–114.
22. Yamaguchi, M., F. Miyamaru, K. Yamamoto, M. Tani, and M. Hangyo. 2005. Terahertz absorption spectra of L-, D-, and DL-alanine and their application to determination of enantiometric composition. *Appl. Phys. Lett.* 86:053903.
23. Shen, S. C., L. Santo, and L. Genzel. 1981. Far infrared spectroscopy of amino acids, polypeptides and proteins. *Can. J. Spectrosc.* 26:126–133.
24. Bandekar, J., L. Genzel, F. Kremer, and L. Santo. 1983. The temperature-dependence of the far-infrared spectra of L-alanine. *Spectrochim. Acta [A].* 39:357–366.
25. Shen, S. C., L. Santo, and L. Genzel. 2007. THz spectra of some biomolecules. *Int. J. Infrared Millim. Waves.* 28:595–610.
26. Yamamoto, K., K. Tominaga, H. Sasakawa, A. Tamura, H. Murakami, H. Ohtake, and N. Sarukura. 2005. Terahertz time-domain spectroscopy of amino acids and polypeptides. *Biophys. J.* 89:L22–L24.
27. Shi, Y., and L. Wang. 2005. Collective vibrational spectra of α- and γ-glycine studied by terahertz and Raman spectroscopy. *J. Phys. D Appl. Phys.* 38:3741–3745.
28. Yu, B., F. Zeng, Y. Yang, Q. Xing, A. Chechin, X. Xin, I. Zeylikovich, and R. R. Alfano. 2004. Torsional vibrational modes of tryptophan studied by terahertz time-domain spectroscopy. *Biophys. J.* 86:1649–1654.
29. Upadhya, P. C., Y. C. Shen, A. G. Davies, and E. H. Linfield. 2003. Terahertz time-domain spectroscopy of glucose and uric acid. *J. Biol. Phys.* 29:117–121.
30. Nishizawa, J.-I., K. Suto, T. Sasaki, T. Tanabe, and T. Kimura. 2003. Spectral measurement of terahertz vibrations of biomolecules using a GaP terahertz-wave generator with automatic scanning control. *J. Phys. D Appl. Phys.* 36:2958–2961.

31. Walther, M., B. M. Fischer, and P. U. Jepsen. 2003. Noncovalent intermolecular forces in polycrystalline and amorphous saccharides in the far infrared. *Chem. Phys.* 288:261–268.

32. Kutteruf, M. R., C. M. Brown, L. K. Iwaki, M. B. Campbell, T. M. Korter, and E. J. Heilweil. 2003. Terahertz spectroscopy of short-chain polypeptides. *Chem. Phys. Lett.* 375:337–343.

33. Shotts, W. J., and A. J. Sievers. 1974. The far-infrared properties of polyamino acids. *Biopolymers.* 13:2593–2614.

34. Yamamoto, K., K. Tominaga, H. Sasakawa, A. Tamura, H. Murakami, H. Ohtake, and N. Sarukaru. 2002. Far-infrared absorption measurements of polypeptides and cytochrome *c* by THz radiation. *Bull. Chem. Soc. Jpn.* 75:1083–1092.

35. Xie, A., Q. He, L. Miller, B. Sclavi, and M. R. Chance. 1999. Low frequency vibrations of amino acid homopolymers observed by synchrotron far-IR absorption spectroscopy: excited state effects dominate the temperature dependence of the spectra. *Biopolymers.* 49:591–603.

36. Powell, J. W., G. S. Edwards, L. Genzel, F. Kremer, A. Wittlin, W. Kubasek, and W. Peticolas. 1987. Investigation of far-infrared vibrational modes in polynucleotides. *Phys. Rev. A.* 35:3929–3939.

37. Strachan, C. J., P. F. Taday, D. A. Newnham, K. C. Gordon, J. A. Zeitler, M. Pepper, and T. Rades. 2005. Using terahertz pulsed spectroscopy to quantify pharmaceutical polymorphism and crystallinity. *J. Pharm. Sci.* 94:837–846.

38. van Exter, M., and D. Grischkowsky. 1990. Characterization of an optoelectronics terahertz beam system. *IEEE Trans. Microw. Theory Tech.* 38:1684–1691.

39. Walther, M., P. Plochocka, B. Fischer, H. Helm, and P. U. Jepsen. 2002. Collective vibrational modes in biological molecules investigated by terahertz time-domain spectroscopy. *Biopolymers.* 67:310–313.

40. Walther, M. 2003. Modern spectroscopy on biological molecules: structure and bonding investigated by THz time-domain and transient phase-grating spectroscopy. Ph.D. Thesis, Albert-Ludwigs-Universität Freiburg, Freiburg, Germany.

41. Frisch M. J., G. W. Trucks, H. B. Schlegel, G. E. Scuseria, M. A. Robb, J. R. Cheeseman, J. A. Montgomery Jr., K. N. Kudin, J. C. Burant, J. M. Millam, S. S. Iyengar, J. Tomasi, V. Barone, B. Mennucci, M. Cossi, G. Scalmani, N. Rega, G. A. Petersson, H. Nakatsuji, M. Hada, M. Ehara, K. Toyota, R. Fukuda, J. Hasegawa, M. Ishida, T. Nakajima, Y. Honda, O. Kitao, H. Nakai, M. Klene, X. Li, J. E. Knox, H. P. Hratchin, J. B. Cross, C. Adamo, J. Jaramillo, R. Gomperts, R. E. Stratmann, O. Yazyev, A. J. Austin, R. Cammi, C. Pomelli, J. W. Ochterski, P. Y. Ayala, K. Morokuma, G. A. Voth, P. Salvador, J. J. Dannenberg, V. G. Zakrzewski, S. Dapprich, A. D. Daniels, M. C. Strain, O. Farkas, D. K. Malik, A. D. Rabuck, K. Raghavachari, J. B. Foresman, J. V. Ortiz, Q. Cui, A. G. Baboul, S. Clifford, J. Cioslowski, B. B. Stefanov, G. Liu, A. Liashenko, P. Piskorz, I. Komaromi, R. L. Martin, D. J. Fox, T. Keith, A. Al-Lahan, C. Y. Peng, A. Nanayakkara, M. Challacombe, P. M. W. Gill, B. Johnson, W. Chen, M. W. Wong, C. Gonzalez, and J. A. Pople. 2003. Gaussian 03, Ver. B.04. Gaussian, Pittsburgh, PA.

42. Berendsen, H. J. C., and S. Hayward. 2000. Collective protein dynamics in relation to function. *Curr. Opin. Struct. Biol.* 10:165–169.

43. Lee, C., K.-H. Park, and M. Cho. 2006. Vibrational dynamics of DNA. I. Vibrational basis modes and couplings. *J. Chem. Phys.* 125:114508.

44. Jepsen, P. U., and S. J. Clark. 2007. Precise ab-initio prediction of terahertz vibrational modes in crystalline systems. *Chem. Phys. Lett.* 442:275–280.

45. Allis, D. G., A. M. Fedor, T. M. Korter, J. E. Bjarnason, and E. R. Brown. 2007. Assignment of the lowest-lying THz absorption signatures in biotin and lactose monohydrate by solid-state density functional theory. *Chem. Phys. Lett.* 440:203–209.

46. Zhang, J., and D. Grischkowsky. 2004. Waveguide THz time-domain spectroscopy of nm water layers. *Opt. Lett.* 19:1617–1619.

47. Melinger, J. S., N. Laman, S. S. Harsha, and D. Grischkowsky. 2006. Line narrowing of terahertz vibrational modes for organic thin polycrystalline films within a parallel plate waveguide. *Appl. Phys. Lett.* 89:251110.

48. Melinger, J. S., N. Laman, S. S. Harsha, and D. Grischkowsky. 2007. High-resolution waveguide terahertz spectroscopy of partially oriented organic polycrystalline films. *J. Phys. Chem. A.* 111:10977–10978.

49. Mendis, R., and D. Grischkowsky. 2001. Undistorted guided wave propagation of sub-picosecond THz pulses. *Opt. Lett.* 26:846–848.

50. Gallot, G., S. P. Jamison, R. W. McGowan, and D. Grischkowsky. 2000. THz waveguides. *J. Opt. Soc. Am. B.* 17:851–863.

51. Laman, N., and D. Grischkowsky. 2007. Reduced conductivity in the terahertz skin-depth layer of metals. *Appl. Phys. Lett.* 90:122115.

52. Aizenberg, J., A. J. Black, and G. M. Whitesides. 1999. Control of crystal nucleation by patterned self-assembled monolayers. *Nature.* 398:495–498.

53. Landau, E. M., M. Levanon, L. Leiserowitz, M. Lahav, and J. Sagiv. 1985. Transfer of structural information from Langmuir monolayers to three-dimensional growing crystals. *Nature.* 318:353–356.

54. Briseno, A. L., J. Aizenberg, Y.-J. Han, R. A. Penkala, H. Moon, A. J. Lovinger, C. Kloc, and Z. Bao. 2005. Patterned growth of large oriented organic semiconductor single crystals on self-assembled monolayer templates. *J. Am. Chem. Soc.* 127:12164–12165.

55. Tao, N. J., J. A. DeRose, and S. M. Lindsay. 1993. Self-assembly of molecular superstructures studied by in-situ scanning tunneling microscopy: DNA bases on Au(111). *J. Phys. Chem.* 97:910–919.

56. Heckl, W. M., D. P. E. Smith, G. Binnig, H. Klagges, T. W. Hänsch, and J. Maddocks. 1991. Two-dimensional ordering of the DNA base guanine observed by scanning tunneling microscopy. *Proc. Natl. Acad. Sci. USA.* 88:8003–8005.

57. Williams, A. J., and V. K. Gupta. 2001. Self-assembly of a rodlike polypeptide on solid surfaces: role of solvent, molecular weight, and time of assembly. *J. Phys. Chem. B.* 105:5223–5230.

58. Chang, Y.-C., and C. W. Frank. 1998. Vapor deposition. Polymerization of α-amino acid N-carboxy anhydride on the silicon (100) native oxide surface. *Langmuir.* 14:326–334.

59. Bamdad, C. 1998. A DNA self-assembled monolayer for the specific attachment of unmodified double- or single-stranded DNA. *Biophys. J.* 75:1997–2003.

60. Endres, R. G., D. L. Cox, and R. R. P. Singh. 2004. Colloquium: the quest for high-conductance DNA. *Rev. Mod. Phys.* 76:195–214.